



Contribution to the Symposium: 'Marine Acoustics Symposium'

Original Article

Remote sensing of habitat characteristics using echo metrics and image-based seabed classes

George R. Cutter, Jr*, Kevin L. Stierhoff, and David A. Demer

Southwest Fisheries Science Center, National Marine Fisheries Service, National Oceanic and Atmospheric Administration, 8901 La Jolla Shores Drive, La Jolla, CA 92037, USA

*Corresponding author: tel: +1 858 546 5691; fax: +1 858 546 7003; e-mail: george.cutter@noaa.gov

Cutter, G. R. Jr, Stierhoff, K. L., and Demer, D. A. Remote sensing of habitat characteristics using echo metrics and image-based seabed classes. – ICES Journal of Marine Science, 73: 1965–1974.

Received 31 August 2015; revised 5 February 2016; accepted 5 February 2016; advance access publication 17 March 2016.

The seabed can be classified using data from vertical, split-beam echosounders. This was demonstrated recently using a model parameterized with acoustic estimates of slope, roughness, normal-incidence backscattering strength, and variation of backscattering strength by frequency and incidence angle. These seabed classifications were interpreted and validated using published surficial geology maps, but the acoustic data indicated greater spatial variability. Here, classifications of sediment grain or feature size are ascribed to areas $\sim 10 \text{ m}^2$. First, images of the seabed in the study area are ascribed, based on per cent coverage, to seven primary classes ranging from mud through high-relief rock, and 25 primary–secondary classes. Then, a refined seabed classifier, based on the acoustic model parameters is trained, using a nearest-neighbours algorithm, on a subset of the class data. The classifier accurately predicts 96% of the primary classes, and 93% of the primary–secondary classes from an independent data subset. These methods should be useful for characterizing, mapping, and quantifying potential seabed habitat domains of demersal fish and benthic invertebrates.

Keywords: acoustic backscatter, benthic, demersal, echosounder, habitat, k nearest neighbours, model, roughness, ROV, slope, supervised classification, validation images.

Introduction

Acoustic seabed classification

Classification and prediction of seabed characteristics commonly involves features of the first (Hamilton, 2014) or first and second seabed echoes measured with single-beam echosounders (Anderson *et al.*, 2008). The features may be correlated with classes of physical or image samples (e.g. Heald and Pace, 1996; Tsehmahman *et al.*, 1997; Zimmermann and Rooper, 2008) to provide seabed classification over large areas. Although single-beam classification models are widely used (Madricardo *et al.*, 2012), the commonly used parameters may not contain sufficient information to accurately characterize seabed (Hamilton, 2014). However, with consideration of the dependence of echo intensity on incidence angle, θ , echo features may more accurately classify sediment grain size and surface roughness (Sternlicht and de Moustier, 2003; van Walree *et al.*, 2006; De and Chakraborty, 2011; Haris *et al.*, 2011). This “angle-response” of the seabed surface backscattering strength,

$S_s(\theta)$, may be measured with multibeam echosounders (e.g. Fonseca and Mayer, 2007; Fonseca *et al.*, 2009; Jackson *et al.*, 2010; Kloser *et al.*, 2010; Lamarche *et al.*, 2011) or split-beam echosounders (Cutter and Demer, 2014). The “frequency-response”, $S_s(f)$, measured with multifrequency or broadband echosounders (Pace and Ceen, 1982; Jia and Courtney, 2001), may further improve seabed classifications. Measures of both the angle- and frequency-response of seabed surface backscattering, $S_s(\theta, f)$, as well as volume backscattering, allow inversion of “geoacoustic” models to predict seabed properties such as grain size, surface porosity and roughness, and volume heterogeneity. Using data from a ship-mounted multi-beam echosounder, such classifications are range-dependent and often have resolutions $\sim 10^3$ – 10^4 m^2 .

Model validation

Acoustic seabed classification requires validation with independent observations ideally having equivalent capability to resolve seabed

features. Validation data are commonly obtained from sediment samples (Hamilton, 2014), underwater images from cameras on human-occupied submersibles (Yoklavich *et al.*, 2000; Anderson and Yoklavich, 2007), towed vehicles (Kloser *et al.*, 2010), or remotely operated vehicles (ROVs) (Nasby-Lucas *et al.*, 2002; Dartnell and Gardner, 2004; Rooper and Zimmermann, 2007; Whitmire *et al.*, 2007; Ierodiaconou *et al.*, 2011; Rattray *et al.*, 2014), or a combination of images and sediment samples (e.g. Dartnell and Gardner, 2004; van Walree *et al.*, 2005). These data typically have much higher resolution, but cover a much smaller portion of the study area compared with the acoustic classes (Kostylev *et al.*, 2001; Dartnell and Gardner, 2004; Kloser *et al.*, 2010; Young *et al.*, 2010; Brown *et al.*, 2011; Lamarche *et al.*, 2011; Todd and Kostylev, 2011; Krigsman *et al.*, 2012). Consequently, the accuracy of the model predictions could be improved by increasing the resolution of the acoustic samples and the coverage of the validation data (Cutter and Demer, 2014).

Split-beam echosounders and multifrequency biplanar interferometric imaging

Cutter and Demer (2010) developed the multifrequency biplanar interferometric imaging technique (MBI) for processing data from multiple-frequency echosounders with overlapping, split-beams. With knowledge of the beam orientations, MBI provides measures of $S_s(\theta, f)$, and estimates of seabed slope and roughness for many samples of the seabed echo received in each beam (Cutter and Demer, 2014). These data, accumulated from a few transmissions along a survey track, may be used to create high-resolution seabed classification models.

Building upon the methods detailed in Demer *et al.* (1999, 2009), Conti *et al.* (2005), and Cutter and Demer (2010), Cutter and Demer (2014) classified the seabed at 43-Fathom Bank in the Southern California Bight (SCB) using metrics derived from MBI processing

of data collected using a calibrated multifrequency (38, 70, 120, and 200 kHz) split-beam echosounder (Simrad EK60). They used measures of $S_s(\theta, f)$ (see Figure 2 in Cutter and Demer, 2014) to solve a log-linear model for normal-incidence backscattering strength (S_{00}) and coefficients for the angle- (C_a) and frequency-dependence (C_f) of S_s . They also evaluated metrics for seabed slope ($\bar{\theta}$) and roughness (\mathcal{R}) distributions.

Cluster analysis of S_{00} , C_a , C_f , $\bar{\theta}$, and \mathcal{R} produced seven seabed classes with attributes determined by their spatial correspondence with features evident from high-resolution bathymetry (Cutter and Demer, 2014) and surficial geological attributes (Goldfinger *et al.*, 2007). Despite the high spatial resolution of the MBI-based metrics, validation of the unsupervised seabed classification model was limited by the low resolution of the surficial geology (Figure 1) (also see Figure 5 of Cutter and Demer, 2014). Consequently, the fine spatial-scale variation in the acoustic parameters, potentially indicative of important seabed habitat features, was necessarily ignored.

Matching scales

In this study, we improve seabed classification using the acoustic model data of Cutter and Demer (2014) by developing and statistically evaluating the performance of a supervised classification model that is trained by independent samples of seabed class from video images collected using an ROV. With this approach, we aim to better match the resolution of model predictions of seabed class to seabed features that comprise habitat for demersal and benthic fish and invertebrates.

Methods

Methods for seabed classification, intended for general application, are developed and their efficacy demonstrated using data from the 43-Fathom Bank, located ~70 km west of San Diego, California.

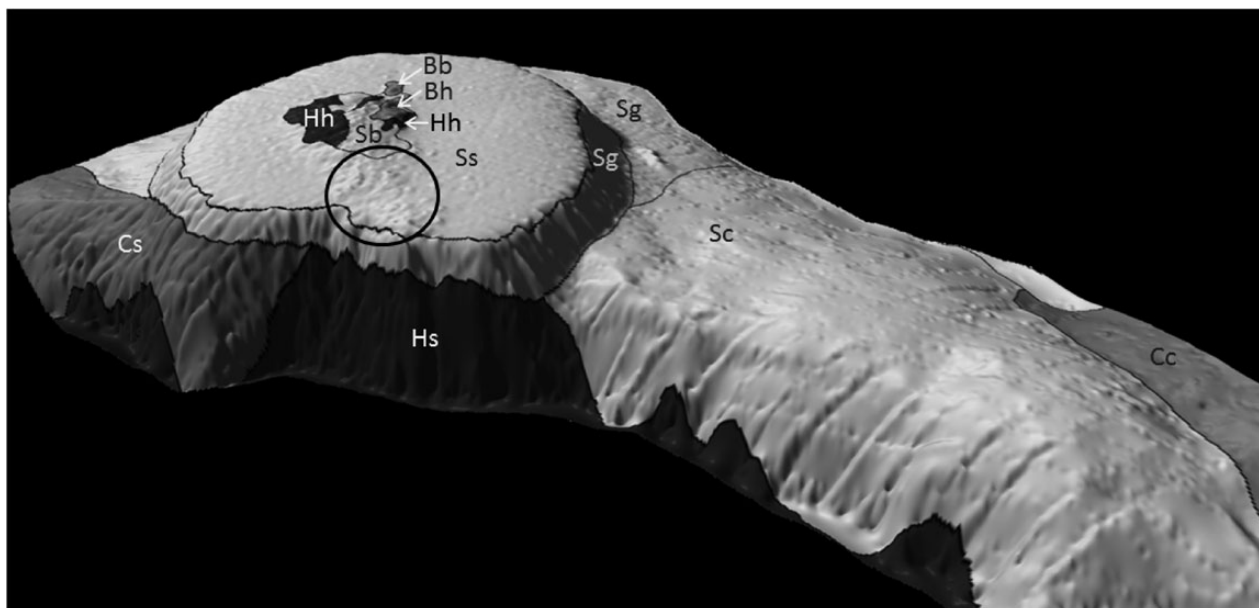


Figure 1. Shaded relief bathymetry map from Cutter and Demer (2014) overlaid with the substrate classes (primary class regions indicated by greyscale level and bounded by lines) and labelled with primary and secondary substrate classes (Ss, sand; Sb, sand and boulder; Sg, sand and gravel/pebble; Sc, sand and cobble; Cs, cobble and sand; Cc, cobble and cobble; Hh, high-relief rock; Hs, high-relief rock and sand; Bb, boulder; Bh, boulder and high-relief rock) in Goldfinger *et al.* (2007). The bathymetry and acoustic model data (see Cutter and Demer, 2014) suggest that there are some misclassifications, e.g. in the circled area, the primary or secondary class is evidently boulder or rock.

The bank was surveyed multiple times, both with echosounders deployed on a ship, and with cameras deployed on a ROV (Demer *et al.*, 2009; Cutter and Demer, 2010, 2014). Earlier results reveal that the top of the bank has a nearly circular terrace at ~ 100 m depth with a high-relief (~ 20 m), rocky peak in the centre that rises to ~ 80 m depth (Figure 2; Cutter and Demer, 2014) that is habitat for a resident rockfish assemblage (Demer *et al.*, 2009).

Acoustic data

The acoustic data for this study were acquired from a calibrated, four-frequency (38, 70, 120, and 200 kHz) split-beam echosounder system (Simrad EK60), using transducers installed in the extendible centreboard of NOAA Fisheries Survey Vessel *Bell M. Shimada* (for more detail, see Cutter and Demer, 2014). As in Cutter and Demer (2014), data from $>66\,000$ transmissions were processed with MBI to estimate values of S_{s0} , C_a , C_f , $\bar{\theta}$, and \mathcal{R} for each 30-transmission ensemble.

Image data

From 2004 through 2012, 37 strip-transect surveys were conducted at 43-Fathom Bank using two different ROVs. Generally, the transect locations and directions were chosen to encounter fish targets observed acoustically, and video images were used to identify fish species and estimate their lengths (Demer *et al.*, 2009). The images were also analysed to ascribe seabed classes. In 2012, several additional transects were conducted specifically to classify the seabed in locations that were not previously sampled (Figure 2).

Transects conducted between 5 March 2004 and 29 October 2010 used a *Phantom* DS4 ROV (Deep Ocean Engineering, Inc.) with a colour-video camera (Sony FCB-IX47C with 468×720 pixel resolution and an $18 \times$ optical zoom). Transects conducted between 17 April 2012 and 29 October 2012 used a custom ROV (HDHV-ROV, NOAA Southwest Fisheries Science Center) with a high-definition video camera [1920×1080 pixel resolution, interlaced (1080i); Mini Zeus, Insite Pacific, Inc.]. Both cameras were mounted on a rotating camera tray. The imaged width varied with the horizontal viewing angle of the camera, the pitch of the camera tray, and the height of the camera above the seabed; the pitch and altitude of the camera may be modulated by the vertical relief of the seabed, the type of survey being conducted, or both. During these surveys, both cameras were oriented $\sim 30^\circ$ below horizontal and ~ 1 m above the seabed. The measured horizontal viewing angle was 50° for the *Phantom* ROV camera and 62° for the HDHV-ROV cameras; consequently, the average imaged width, estimated based on the camera altitude, pitch, and horizontal viewing angle, was 2.6 and 4.4 m for the *Phantom* and HDHV-ROV cameras, respectively. Two parallel laser calipers (spaced 20 and 61 and 40 cm apart on the *Phantom* and HDHV ROVs, respectively) provided a constant measurement scale that analysts used to judge feature sizes for describing seabed class. All video footage was recorded to digital video (DV) tape (DVCAM or HDV format for standard and high-definition video, respectively) and later used for characterizing the seabed. ROV positions were estimated using an ultra-short baseline (USBL) acoustic tracking system (Track-Point II-Plus, ORE Offshore for the *Phantom* ROV; TrackLink 5000, LinkQuest, Inc. for

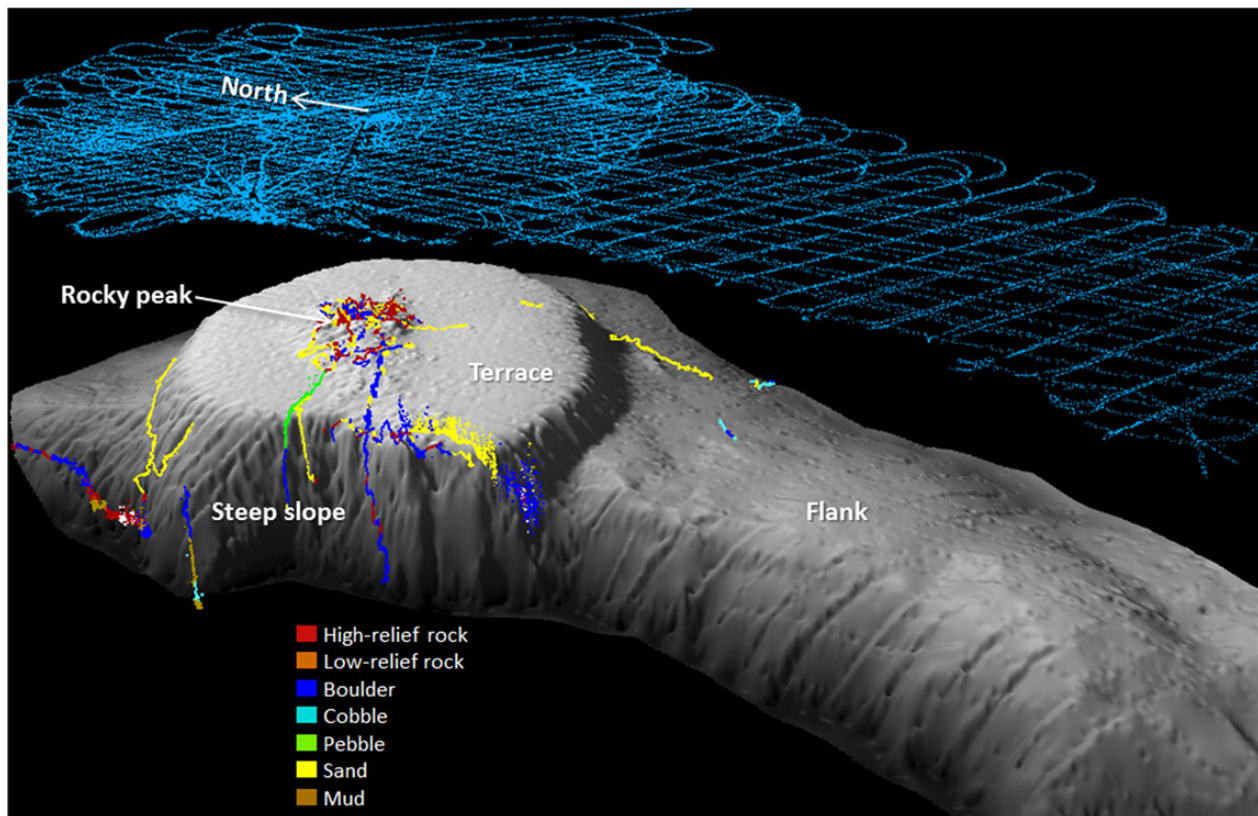


Figure 2. The 43-Fathom Bank study area, viewed from the southwest, with acoustic-survey tracklines (above) and ROV transects [symbolized by the primary seabed classes (C_p) observed in video images] on the acoustically mapped bathymetry surface.

the HDHV-ROV) and differential global positioning system (dGPS, CSI Wireless dGPS MAX). The length of each transect was estimated from the speed of the ROV, which was measured using a Doppler velocity log (DVL; Workhorse Navigator, Teledyne RD Instruments). All data were time-stamped and logged synchronously using integrated navigation software (WinFrog, Fugro Pelagos, Inc.). ROV positions estimated from the USBL systems were smoothed using a Kalman filter to eliminate bad navigation system observations and artefacts of sudden apparent shifts of position.

Image analysis

Approximately 57 000 video images of the seabed, collected every ~ 1 – 2 s along the ROV transects, separated by ~ 0.1 – 4.3 m, were visually classified. Classifications were made at the beginning of each transect, changed according to perceived changes in the seabed composition [similar to Stein *et al.* (1992) and dynamic segmentation in a GIS (Esri, 1994)], and checked by a second analyst. The classes are based on sediment grain size (Wentworth, 1922; Folk, 1974) and relief for bedrock outcrops. The classes correspond to the “seabed substrate” classes of the scheme used by Goldfinger *et al.* (2007). The classes are: mud (M, <0.06 mm), sand (S, 0.06 – 2 mm), pebble (P, 2 – 64 mm), cobble (C, 64 – 256 mm), boulder (B, 0.25 – 3 m), low-relief rock (L, <0.25 m), and high-relief rock (H, >0.25 m) such that rock classes are distinct from boulders by their spatial continuity. Primary classes, C_p , designated by a capital letter, comprise the majority of the area within a seabed

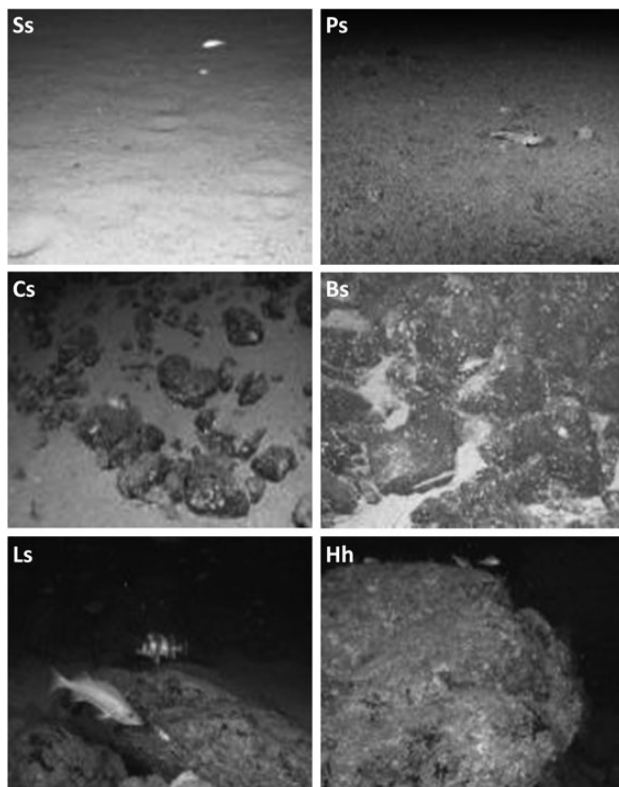


Figure 3. Examples of ROV images with visually identified seabed classes (defined in Table 2) observed at the 43-Fathom Bank. Labels indicate primary–secondary seabed class (C_{ps}) with the primary (C_p) capitalized and secondary (C_s) in lower case.

image (Figure 3); secondary classes, C_s , designated by a lower-case letter, comprise a minority of the imaged area. Combined primary and secondary seabed classes (Tables 1 and 2), C_{ps} , are designated by upper- and lower-case letter combinations, e.g. $C_{ps} = Sc$ for images with mostly sand and some cobble.

Classification

Assigning seabed classes to acoustic metrics for supervised classification

For the supervised classification of the seabed, we developed a classifier trained using spatially coincident acoustic-model data and image-based seabed class data. Within a random subset of the full dataset, acoustic metrics, S_{s0} , C_a , C_f , $\bar{\theta}$, and \mathcal{R} , defined in Cutter and Demer (2014) were collected within each homogenous area, $A_h = \pi R_h^2$, where the homogeneity radius, R_h , is the maximum value, ≤ 30 m, for which all C_p are the same (Figure 4). Training subsets from 10 to 50% of the full dataset were tested, but 30% (9275 observations) was ultimately used. Subsets were generated by iterative resampling of the full dataset until each C_p or C_{ps} was represented by at least six observations. Generally, the subsets included more than 20 images with mud and many more of the other classes. The median values ($\text{med}[\]$) of the acoustic metrics within each A_h comprise a class-feature vector, V ,

$$V = \{\text{med}[C_f], \text{med}[C_a], \text{med}[S_{s0}], \text{med}[\mathcal{R}], \text{med}[\bar{\theta}]\}.$$

k -nearest neighbours classifier

A k -nearest neighbours (kNN) classifier model (Duda *et al.*, 2001) was used to predict C_p and C_{ps} values (\widehat{C}_p and \widehat{C}_{ps}) and for each of the feature vectors in the testing subset, based on a majority voting scheme and their k nearest neighbours, according to the Mahalanobis distance in the multi-variate space of the acoustic metrics. The Mahalanobis distance, which incorporates the covariance of V (Davis, 1986), was used instead of the Euclidean distance because it provided better prediction accuracies for \widehat{C}_p and \widehat{C}_{ps} (comparison not shown). Values of k from 1 to 500 were tested, but the optimal value was 1. All five features, i.e. each acoustic metric, passed the sequential floating forward selection (SFFS) method (Pudil *et al.*, 1994), as implemented by Pohjalainen *et al.*, (2015) and were retained for classification. Training and prediction of \widehat{C}_p and \widehat{C}_{ps} were done independently.

Performance evaluation and prediction

Uncertainty in the \widehat{C}_p and \widehat{C}_{ps} were assessed by comparisons with the C_p and C_{ps} indicated by the ROV images in the test subset. Overall prediction accuracy (p_{acc}) and error (p_{err}) were estimated by iteratively generating new random training and test subsets. Additionally, a fourfold cross-validation was used to provide an alternative estimate of p_{err} . The cross-validated kNN model was then used to predict \widehat{C}_p and \widehat{C}_{ps} for the acoustic metrics in the entire dataset. The most frequent class (mode) and number of classes of \widehat{C}_p and \widehat{C}_{ps} within 50-by-50 m grid cells were calculated for the entire study area.

Results

Seabed class

A total of 57 859 assignments of primary (C_p), secondary (C_s), and primary–secondary seabed class (C_{ps}) were obtained from the ROV’s video imagery. Sand, boulder, and high-relief rock were the

Table 1. Summary of video image seabed classifications: overall frequency, and percentage (in parentheses) of primary (C_p) and secondary class (C_s) (total $n = 57\ 859$).

Level	Class						
	Mud (M)	Sand (S)	Pebble (P)	Cobble (C)	Boulder (B)	Low-relief rock (L)	High-relief rock (H)
C_p	909 (1.6)	24 805 (42.9)	838 (1.4)	2530 (4.4)	18 161 (31.4)	1344 (2.3)	9272 (16.0)
C_s	3903 (6.7)	28 367 (49.0)	1028 (1.8)	1755 (3.0)	17 694 (30.6)	1011 (1.7)	4101 (7.1)

Table 2. Percentages of 57 859 primary–secondary classes (C_{ps}) from video images of the seabed at the 43-Three Fathom Bank.

Primary class	Secondary class							
	Mud (m)	Sand (s)	Pebble (p)	Cobble (c)	Boulder (b)	Low-relief rock (l)	High-relief rock (h)	Total
Mud (M)	0.0	0.0	0.0	0.3	1.3	0.0	0.0	1.6
Sand (S)	0.0	30.0	1.6	0.5	8.2	0.2	2.4	42.9
Pebble (P)	0.0	1.3	0.1	0.0	0.0	0.0	0.0	1.4
Cobble (C)	0.2	0.1	0.0	1.2	2.8	0.0	0.0	4.4
Boulder (B)	4.8	11.3	0.0	0.9	14.2	0.1	0.2	31.4
Low-relief rock (L)	0.4	0.3	0.0	0.0	0.1	1.5	0.0	2.3
High-relief rock (H)	1.2	6.2	0.0	0.1	4.4	0.0	4.2	16.0
Total	6.6	49.4	1.7	2.8	31.0	1.7	6.7	100

Primary class (C_p) is capitalized and secondary class (C_s) is lower case.

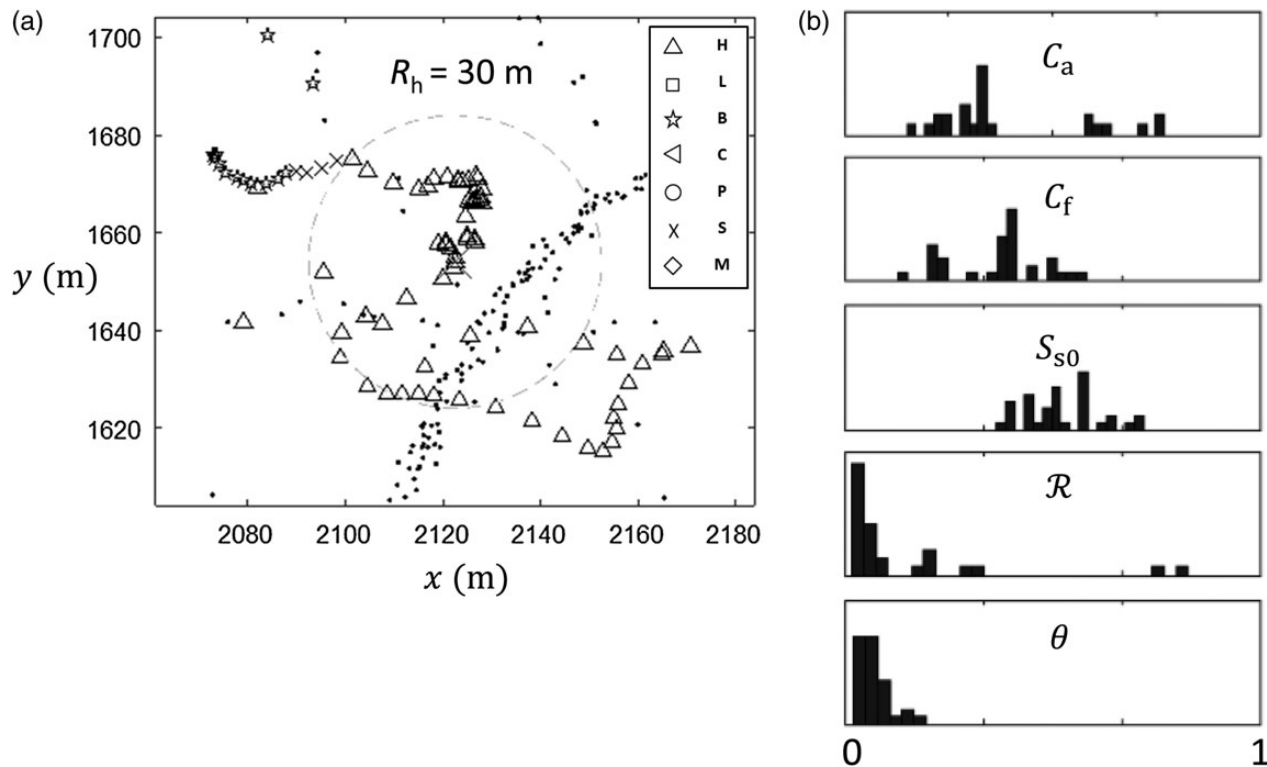


Figure 4. (a) Echosounder (dots) and ROV-video image samples (symbolized by C_p ; refer to Table 2 for symbol codes) at 43-Fathom Bank. The dashed circle indicates the area of homogeneity (A_h) defined by radius (R_h), within which the primary class (C_p) of all image samples is the same (H, in this case). (b) Distributions of the acoustically derived metrics within A_h : coefficients for the angle- (C_a) and frequency-response (C_f) of S_s ; normal-incidence backscattering strength (S_{s0}); roughness (\mathcal{R}); and slope (θ) (for details, see Cutter and Demer, 2014).

most commonly observed primary and secondary classes (Table 1). Four of the 29 observed C_{ps} classes were combined (\rightarrow) with similar classes, resulting in 25 C_{ps} classes (Table 2) because of few (< 60) observations ($Lb \rightarrow Ll$, $Hc \rightarrow Hb$, $Bl \rightarrow Bb$) or to avoid potential

misclassification of C_s as mud ($Lm \rightarrow Ls$). This causes slight differences in the percentage of C_s in Table 1 and column totals in Table 2. Also, note that not all primary–secondary combinations were observed (Table 2).

Characteristic distance

For many areas outside of the rocky peak region, R_h was at least 30 m, the largest radius tested, and consistent throughout entire ROV transects, indicating homogeneous seabed class and gradual spatial variation. However, within the rocky regions, many images had R_h values of 0 m (indicating that the value only applied to a single location) to 2 m, indicating high heterogeneity or a transition.

Predicted seabed class

The geographic distribution of the seven predicted primary classes, \widehat{C}_p , was mostly consistent with the results of previous studies of the seabed geology at 43-Fathom Bank (Goldfinger et al., 2007; Cutter and Demer, 2014). Sand was the most common \widehat{C}_p , particularly on the terrace (Figure 5). The rocky peak comprises predominantly high- (H) and low-relief rock (L) and boulder (B). The surrounding terrace is mostly sand (S) and some pebble (P). The deeper south-eastern flank is mostly cobble (C) with patches of sand. The small,

deep area on the northwest flank includes cobble. The steep slope along the western edge of the bank is mostly boulder. There is mud (M) in only a few locations on this steep slope. High-relief rock extends from the central peak to the south, and down the steep western slope.

The 25 predicted primary–secondary classes, \widehat{C}_{ps} , were dominated by Ss (Figure 5), which covered most of the flat terrace. The terrace flats also contained Pp and Ps. The rocky peak area, and the adjacent area extending to the south-southwest off the western edge of the bank were composed of Hh, Hb, Hs, and Bb. The steep western slope of the bank was mostly Bb. The deep flank in the southeastern part of the study area included mostly Cb, Cc, and Cs.

The modal \widehat{C}_p of the rocky peak is predominately H and B, with a moderate diversity (the number of primary classes in each 50-m grid cell) of 3–4. The eastern-southeastern edge of the rocky peak has areas of higher diversity, 5–6, and steep slope in the southwest has the highest diversity, 6–7 classes per cell.

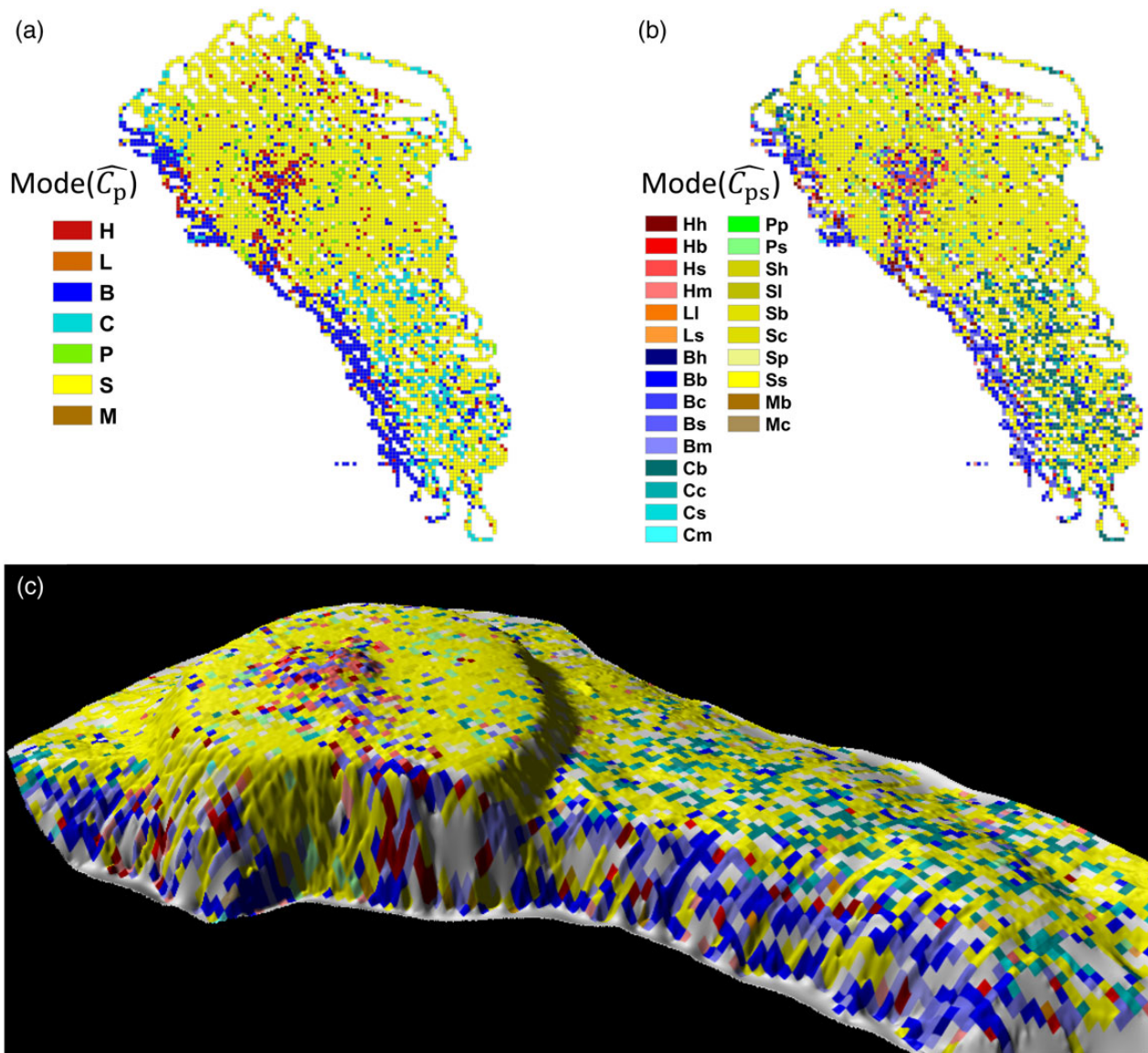


Figure 5. Mode of predicted seabed classes (a) \widehat{C}_p and (b) \widehat{C}_{ps} , within 50-by-50 m grid cells for the entire study area, and (c) \widehat{C}_{ps} overlaid on the shaded-relief bathymetry surface (legend for b applies to c); white cells indicate no data.

The modal \widehat{C}_{ps} of the rocky peak is dominated by Hb, Hs, Bs, Bc, Bb, and Hh and has high diversity ($>8 \widehat{C}_{ps}$ classes per cell) along the east-southeast edge. The terrace is principally Ss with low diversity, 1–4 classes per cell, and the deep southeast flank has large patches of Cb and Cc with generally low to moderate diversity. The steep western slope is mostly Bb, except in two deep locations where there are large patches of Hh. The steep slope to the southwest and a deep area off the northwest of the bank have large regions of high diversity with >8 classes per cell.

Areal coverage of the \widehat{C}_p , based on the modal \widehat{C}_p grid, is highly variable, for example, sand accounts for 68% (10 km²), boulder 15% (2.3 km²), high-relief rock 4.5% (0.7 km²), and mud only 0.05% (0.008 km²) (Table 3). For modal \widehat{C}_{ps} , Ss is most common, accounting for 57% (9 km²), followed by Bb (7.6%, 1.2 km²), Cb

(7.5%, 1.1 km²), Bs (5.5%, 0.8 km²), and Cc (2.6%, 0.4 km²) (Table 3). Sb, Ps, and Hs each cover just over 2% (0.3–0.4 km²).

Classifier performance

Sensitivity to classifier parameters

Classifier performance varied with classifier parameters, particularly k and the distance metric. The accuracy of the kNN classifier decreased with increasing k . As k increased from 1 to 10, the accuracy of the kNN classifier decreased from 96 to 89% for \widehat{C}_p and from 93 to 83% for \widehat{C}_{ps} (Table 4). The decrease was asymptotic, and stabilized at $\sim 70\%$ for $k \geq 200$. Compared with results using the Mahalanobis distance, using the Euclidean distance resulted in prediction accuracy that was lower by $\sim 1\%$ for $k = 1$ to 2.5% for $k = 10$.

The kNN classifier performance was best using $k = 1$ and using the Mahalanobis distance. Based on application to the test (holdout) subsets, the classifications had a mean accuracy of 96% (4% error) for \widehat{C}_p and 93% (7% error) for \widehat{C}_{ps} . N -fold cross-validation errors, 5% for \widehat{C}_p and 7% for \widehat{C}_{ps} , were slightly higher than the holdout errors (Table 5).

Each new run of the classifier entails selection of a new random test and training subset from the total dataset. As such, the classifier performance varies slightly with each run. For >100 classifier iterations, the test-set classification error was 3.9% (standard deviation = 0.2%).

Contingency table analysis

Although the overall prediction accuracy, estimated using the holdout method, was 96% correct, the prediction accuracy for each class ranged from ~ 89 to 98% (Table 5) but varied for each realization of the model run for different subsets. In the example presented, the worst case, H had 6% misclassified as S and 5% as B. The best accuracies were for S and C, each with only 2% misclassified. Most of the few misclassification of S were erroneously attributed to M, but some were linked with each of the other classes. A few M (5%) were misclassified as B or H. Rarely was C incorrectly predicted to be S or B, and only once misclassified as M. A total of 4% of B were misclassified as S, C, L, or H. Except for M, each of the other classes were occasionally misclassified as S. This is because the 43-Fathom Bank has large areas of sand, and areas with rock and boulder are in proximity to sand.

Discussion

Accurate definition of the locations and extents of seabed habitats could greatly reduce uncertainty of fishery-independent population

Table 3. Coverage area of modal \widehat{C}_p and \widehat{C}_{ps} based on 50 m grid-cell map.

Primary	Area (%)	Primary – secondary	Area (%)
M	0.05	Mc	0.03
		Mb	0.13
S	67.9	Ss	59.61
		Sp	1.67
		Sc	1.29
		Sb	2.28
		Sl	0.65
		Sh	1.84
P	2.4	Ps	2.30
		Pp	0.08
C	9.7	Cm	0.10
		Cs	0.26
		Cc	2.58
		Cb	7.45
B	15.1	Bm	1.11
		Bs	5.51
		Bc	0.07
		Bb	7.61
		Bh	0.08
L	0.5	Ls	0.36
		Ll	0.30
H	4.5	Hs	2.12
		Hm	0.58
		Hb	0.61
		Hh	1.36

Total coverage area is 15.1 km². Because training and prediction of \widehat{C}_p and \widehat{C}_{ps} were done independently, summed per cent areas of \widehat{C}_{ps} may differ from per cent \widehat{C}_p .

Table 4. Accuracy, holdout error, and cross-validation error for the kNN classifications of primary (\widehat{C}_p) and primary – secondary classes (\widehat{C}_{ps}) in the training set using the Mahalanobis distance and for $k = 1:10$.

k	\widehat{C}_p			\widehat{C}_{ps}		
	Accuracy	Holdout error	Cross-validation error	Accuracy	Holdout error	Cross-validation error
1	0.962	0.038	0.049	0.934	0.066	0.072
2	0.945	0.055	0.068	0.915	0.085	0.102
3	0.941	0.059	0.069	0.906	0.094	0.109
4	0.930	0.070	0.087	0.896	0.104	0.125
5	0.923	0.077	0.092	0.882	0.118	0.139
6	0.915	0.085	0.104	0.872	0.128	0.148
7	0.911	0.089	0.112	0.860	0.140	0.163
8	0.900	0.100	0.118	0.850	0.150	0.169
9	0.896	0.104	0.123	0.845	0.155	0.174
10	0.892	0.108	0.133	0.837	0.163	0.182

Table 5. Known (C_p) vs. predicted (\hat{C}_p) primary seabed classes (% by row) (see Tables 1 and 2 for definitions).

	Predicted						
	M	S	P	C	B	L	H
Known							
M	<i>94.9</i>	0.0	0.0	0.0	1.7	0.0	3.4
S	0.0	<i>97.9</i>	0.2	0.1	0.8	0.1	0.9
P	0.0	7.7	<i>90.8</i>	0.0	1.5	0.0	0.0
C	0.1	1.1	0.0	<i>97.6</i>	1.2	0.0	0.0
B	0.0	2.2	0.0	0.2	<i>95.8</i>	0.4	1.4
L	0.0	2.1	0.0	0.0	2.7	<i>95.2</i>	0.0
H	0.1	5.6	0.0	0.1	4.9	0.4	<i>88.9</i>

Values along the diagonal (italicized) indicate a total of 95% correct predictions for 21 640 observations in the validation subset for this realization of the model.

estimates of groundfish, and thereby improve the assessment and management of rockfish (genus *Sebastes*) and other species. This can be achieved efficiently using remote sensing methods such as acoustics, images collected with an ROV, and the methods and results of this study. Compared with unsupervised classification of echoes, which may be a tenuous proxy for seabed class (Hamilton, 2011), our supervised classification method, trained using a large image dataset, provides a reliable basis for delineating surficial geological attributes of groundfish habitats. Images are used because physical sample collection and processing is time-consuming and expensive, and there is uncertainty in the exact location of a sample relative to an acoustic beam footprint. Furthermore, thousands of seabed images were obtained from each ROV transect, and although they provide less detailed information about the substrate, they better discriminate features important to groundfish habitats.

Notwithstanding the advantages of seabed imaging over other validation methods, seabed classes may be misidentified (Rattray et al., 2014). Image classifications may be biased by serial viewing, feature scale, image-sensor resolution, lighting and orientation, and distance from the camera to the seabed. For example, differences in small grain sizes may not be visually discriminable. Pebbles may be obscured by sand. Large boulders may be indistinguishable from some low-relief rock. Seabed properties may vary within A_h , defined only with respect to C_p , because of variation of the secondary class C_s or proportional coverage of C_p .

If the classification scheme does not allow for an “other” class group value, then all of the images and classifier predictions will be assigned to one of the defined, but perhaps incorrect classes. With recognition of the estimation uncertainty (Table 4), our new map of seabed classes at the 43-Fathom Bank (Figure 5) can form the basis of a high spatial-resolution map of rockfish habitat.

Grain size and relief are important to habitats of many benthic and demersal organisms and can be sensed remotely using our methods. Despite the significant advances facilitated by these methods, the seabed classes in this analysis do not represent all of the habitat characteristics that are important to the infauna, epifauna, flora, or the demersal fish. For example, sand or gravel may be composed of eroded quartz or fragmented bivalve-shells, which comprise substrates that host different benthic faunal assemblages and attract different predators. Other factors, including dissolved oxygen and chlorophyll *a* concentrations, and salinity (Juan-Jorda et al., 2009), epifauna and infauna (Thompson et al., 2001; e.g. Krigsman et al., 2012), and water depth (Love et al.,

2009), are important for habitat characterization but were not considered for this study. However, because our principal species of interest are rockfish, many of which are associated with high- and low-relief rock and boulders (Anderson and Yoklavich, 2007; Love et al., 2009; Young et al., 2010), subtle differences in fine-grained sediments are not critical for this study. However, these sediment types may be important for benthic infauna, which could in turn be important to rockfish habitat. Our method should be able to discriminate among the fine-grained sediments when spatial coverage and training data sufficiently represent those conditions.

Conclusion

We developed a unique method for the prediction of surficial seabed classes using data from hull-mounted, vertically oriented fisheries echosounders (4-frequency EK60) processed using the MBI imaging technique and fit to a simple model of acoustic backscatter by frequency and incidence angle; then using a simple, five-feature classifier that was validated using classified images collected by an ROV. The classification resulted in >95 and >90% prediction accuracy, for 7 primary and 25 primary–secondary seabed classes. The map of modal primary–secondary seabed classes (Figure 5) provides more detail about previously unresolved seabed features at 43-Fathom Bank that may be important habitat for rockfish. Employed on a broader scale, our method could refine prediction of seabed habitat distributions for other fish and invertebrate species, and possibly improved population estimates by incorporating more precise seabed class and habitat information into survey design, by focusing sampling effort in appropriate habitat, and analysis, by refining estimates of habitat area used to calculate abundance from estimates of density.

References

- Anderson, J. T., Holliday, D. V., Kloser, R., Reid, D. G., and Simard, Y. 2008. Acoustic seabed classification: current practice and future directions. *ICES Journal of Marine Science*, 65: 1004–1011.
- Anderson, T. J., and Yoklavich, M. M. 2007. Multiscale habitat associations of deepwater demersal fishes off central California. *Fishery Bulletin*, 105: 168–179.
- Brown, C. J., Todd, B. J., Kostylev, V. E., and Pickrill, R. A. 2011. Image-based classification of multibeam sonar backscatter data for objective surficial sediment mapping of Georges Bank, Canada. *Continental Shelf Research*, 31: S110–S119.
- Conti, S. G., Demer, D. A., Soule, M. A., and Conti, J. H. E. 2005. An improved multiple-frequency method for measuring in situ target strengths. *ICES Journal of Marine Science*, 62: 1636–1646.
- Cutter, G. R., and Demer, D. A. 2010. Multifrequency biplanar interferometric imaging. *IEEE Geoscience and Remote Sensing Letters*, 7: 171–175.
- Cutter, G. R., and Demer, D. A. 2014. Seabed classification using surface backscattering strength versus acoustic frequency and incidence angle measured with vertical, split-beam echosounders. *ICES Journal of Marine Science*, 71: 882–894.
- Dartnell, P., and Gardner, J. V. 2004. Predicting seafloor facies from multibeam bathymetry and backscatter data. *Photogrammetric Engineering and Remote Sensing*, 70: 1081–1091.
- Davis, J. C. 1986. *Statistics and Data Analysis in Geology*. John Wiley and Sons, Hoboken, NJ. 646 pp.
- De, C., and Chakraborty, B. 2011. Model-based acoustic remote sensing of seafloor characteristics. *IEEE Transactions on Geoscience and Remote Sensing*, 49: 3868–3877.
- Demer, D. A., Cutter, G. R., Renfree, J. S., and Butler, J. L. 2009. A statistical-spectral method for echo classification. *ICES Journal of Marine Science*, 66: 1081–1090.

- Demer, D. A., Soule, M. A., and Hewitt, R. P. 1999. A multiple-frequency method for potentially improving the accuracy and precision of in situ target strength measurements. *Journal of the Acoustical Society of America*, 105: 2359–2376.
- Duda, R. O., Hart, P. E., and Stork, D. G. 2001. *Pattern Classification*, 2nd ed. Wiley-Interscience, Hoboken, NJ, USA.
- Esri. 1994. Dynamic segmentation. *In* *Network Analysis*, p. 263. Environmental Systems Research Institute, Inc., Redlands, CA.
- Folk, R. L. 1974. *Petrology of Sedimentary Rocks*. Hemphill Publishing Co., Austin, TX.
- Fonseca, L., Brown, C., Calder, B., Mayer, L., and Rzhano, Y. 2009. Angular range analysis of acoustic themes from Stanton Banks Ireland: a link between visual interpretation and multibeam echosounder angular signatures. *Applied Acoustics*, 70: 1298–1304.
- Fonseca, L., and Mayer, L. 2007. Remote estimation of surficial seafloor properties through the application angular range analysis to multibeam sonar data. *Marine Geophysical Research*, 28: 119–126.
- Goldfinger, C., Romsos, C., Chaytor, J., Yoklavich, M., Amend, M., Watters, D., Wakefield, W. W., et al. 2007. Multibeam sonar surveys and geological habitat mapping of the seafloor within the Cowcod Conservation Areas (CCA), southern California continental borderland. Cooperative Research Report, Oregon State University and National Oceanic and Atmospheric Administration, ATSMR Report 07-01: 40.
- Hamilton, L. 2011. Acoustic seabed segmentation for echosounders through direct statistical clustering of seabed echoes. *Continental Shelf Research*, 31: 2000–2011.
- Hamilton, L. J. 2014. Real-time echosounder based acoustic seabed segmentation with two first echo parameters. *Methods in Oceanography*, 11: 13–28.
- Haris, K., Chakraborty, B., De, C., Prabhudesai, R. G., and Fernandes, W. 2011. Model-based seafloor characterization employing multibeam angular backscatter data—a comparative study with dual-frequency single beam. *Journal of the Acoustical Society of America*, 130: 3623–3632.
- Heald, G. J., and Pace, N. G. 1996. An analysis of 1st and 2nd backscatter for seabed classification. *In* *Proceedings of III European Conference on Underwater Acoustics*, pp. 649–654. Crete.
- Ierodiaconou, D., Monk, J., Rattray, A., Laurenson, L., and Versace, V. L. 2011. Comparison of automated classification techniques for predicting benthic biological communities using hydroacoustics and video observations. *Continental Shelf Research*, 31: S28–S38.
- Jackson, D. R., Odom, R. I., Boyd, M. L., and Ivakin, A. N. 2010. A geoaoustic bottom interaction model (GABIM). *IEEE Journal of Oceanic Engineering*, 35: 603–617.
- Jia, Y., and Courtney, R. C. 2001. Broad-band frequency and incident-angle dependence of bottom backscattering on Browns bank. *IEEE Journal of Oceanic Engineering*, 26: 373–382.
- Juan-Jorda, M. J., Barth, J. A., Clarke, M. E., and Wakefield, W. W. 2009. Groundfish species associations with distinct oceanographic habitats in the Northern California Current. *Fisheries Oceanography*, 18: 1–19.
- Kloser, R. J., Penrose, J. D., and Butler, A. J. 2010. Multi-beam backscatter measurements used to infer seabed habitats. *Continental Shelf Research*, 30: 1772–1782.
- Kostylev, V. E., Todd, B. J., Fader, G. B. J., Courtney, R. C., Cameron, G. D. M., and Pickrill, R. A. 2001. Benthic habitat mapping on the Scotian Shelf based on multibeam bathymetry, surficial geology and sea floor photographs. *Marine Ecology Progress Series*, 219: 121–137.
- Krigsman, L. M., Yoklavich, M. M., Dick, E. J., and Cochrane, G. R. 2012. Models and maps: predicting the distribution of corals and other benthic macro-invertebrates in shelf habitats. *Ecosphere*, 3: 1–16.
- Lamarche, G., Lurton, X., Verdier, A. L., and Augustin, J. M. 2011. Quantitative characterisation of seafloor substrate and bedforms using advanced processing of multibeam backscatter—application to Cook Strait, New Zealand. *Continental Shelf Research*, 31: S93–S109.
- Love, M., Yoklavich, M., and Schroeder, D. 2009. Demersal fish assemblages in the Southern California Bight based on visual surveys in deep water. *Environmental Biology of Fishes*, 84: 55–68.
- Madricardo, F., Tegowski, J., and Donnici, S. 2012. Automated detection of sedimentary features using wavelet analysis and neural networks on single beam echosounder data: a case study from the Venice Lagoon, Italy. *Continental Shelf Research*, 43: 43–54.
- Nasby-Lucas, N. M., Embley, B. W., Hixon, M. A., Merle, S. G., Tissot, B. N., and Wright, D. J. 2002. Integration of submersible transect data and high-resolution multibeam sonar imagery for a habitat-based groundfish assessment of Heceta Bank, Oregon. *Fishery Bulletin*, 100: 739–751.
- Pace, N. G., and Ceen, R. V. 1982. Seabed classification using the backscattering of normally incident broadband acoustic pulses. *Hydrographic Journal*, 26: 9–16.
- Pohjalainen, J., Rasanen, O., and Kadioglu, S. 2015. Feature selection methods and their combinations in high-dimensional classification of speaker likability, intelligibility and personality traits. *Computer Speech and Language*, 29: 145–171.
- Pudil, P., Novovicova, J., and Kittler, J. 1994. Floating search methods in feature selection. *Pattern Recognition Letters*, 15: 1119–1125.
- Rattray, A., Ierodiaconou, D., Monk, J., Laurenson, L. J. B., and Kennedy, P. 2014. Quantification of spatial and thematic uncertainty in the application of underwater video for benthic habitat mapping. *Marine Geodesy*, 37: 315–336.
- Rooper, C. N., and Zimmermann, M. 2007. A bottom-up methodology for integrating underwater video and acoustic mapping for seafloor substrate classification. *Continental Shelf Research*, 27: 947–957.
- Stein, D. L., Tissot, B. N., Hixon, M. A., and Barss, W. 1992. Fish-habitat associations on a deep reef at the edge of the Oregon continental shelf. *Fishery Bulletin*, 90: 540–551.
- Sternlicht, D. D., and de Moustier, C. P. 2003. Remote sensing of sediment characteristics by optimized echo-envelope matching. *Journal of the Acoustical Society of America*, 114: 2727–2743.
- Thompson, A. R., Petty, J. T., and Grossman, G. D. 2001. Multi-scale effects of resource patchiness on foraging behaviour and habitat use by longnose dace *Rhinichthys cataractae*. *Freshwater Biology*, 46: 145–160.
- Todd, B. J., and Kostylev, V. E. 2011. Surficial geology and benthic habitat of the German Bank seabed, Scotian Shelf, Canada. *Continental Shelf Research*, 31: S54–S68.
- Tshmahman, A. S., Collins, W. T., and Prager, B. T. 1997. Acoustic seabed classification and correlation analysis of sediment properties by QTC view. *In* *Proceedings of IEEE OCEANS '97*, pp. 921–926. Halifax, Nova Scotia.
- van Walree, P. A., Ainslie, M. A., and Simons, D. G. 2006. Mean grain size mapping with single-beam echo sounders. *Journal of the Acoustical Society of America*, 120: 2555.
- van Walree, P. A., Tegowski, J., Laban, C., and Simons, D. G. 2005. Acoustic seafloor discrimination with echo shape parameters: a comparison with the ground truth. *Continental Shelf Research*, 25: 2273–2293.
- Wentworth, C. K. 1922. A scale of grade and class terms for clastic sediments. *Journal of Geology*, 30: 377–392.
- Whitmire, C. E., Embley, R. W., Wakefield, W. W., Merle, S. G., and Tissot, B. N. 2007. A quantitative approach for using multibeam sonar data to map benthic habitats. *In* *Mapping the Seafloor for Habitat Characterization: Geological Association of Canada, Special Paper 47*, pp. 111–126. Ed. by B. J. Todd, and H. G. Greene. Geological Association of Canada, St. Johns, Newfoundland.

- Yoklavich, M. M., Greene, H. G., Cailliet, G. M., Sullivan, D. E., Lea, R. N., and Love, M. S. 2000. Habitat associations of deep-water rockfishes in a submarine canyon: an example of a natural refuge. *Fishery Bulletin*, 98: 625–641.
- Young, M. A., Iampietro, P. J., Kvitek, R. G., and Garza, C. D. 2010. Multivariate bathymetry-derived generalized linear model accurately predicts rockfish distribution on Cordell Bank, California, USA. *Marine Ecology Progress Series*, 415: 247–261.
- Zimmermann, M., and Rooper, C. N. 2008. Comparison of echogram measurements against data expectations and assumptions for distinguishing seafloor substrates. *Fishery Bulletin*, 106: 293–304.

Handling editor: Howard Browman